Nonlinear estimation of El Niño impact on the North Atlantic winter

M. J. OrtizBeviá,[1] I. Pérez-González,[1] F. J. Alvarez-García,[1] and A. Gershunov[2]

Received 20 October 2009; revised 3 March 2010; accepted 4 August 2010; published 11 November 2010.

[1] The differences in the teleconnections forced by different El Niño events (Niños) can be partly explained by the intrinsic nonlinearity of the atmospheric response. In the present study, we segregate the responses of the North Atlantic to strong from those to moderate Niños and compare nonlinear and linear estimates. El Niño forcing is represented by the tropical Pacific sea surface temperature anomalies, and the North Atlantic atmospheric response is represented by sea level pressure anomalies in the region. To gain insight into the evolution of El Niño teleconnections in a future climate, linear and nonlinear analyses are carried out on the corresponding data fields in the control and scenario simulations of a climate model experiment. This experiment presents, in its control version, realistic teleconnections. In the observational analysis, the nonlinear method performs only slightly better than the linear one. However, in the analysis of the interannual variability by a long control experiment of a realistic climate simulation, the nonlinear estimate improves significantly with respect to the linear one. The analysis of the corresponding scenario experiment points to an intensification of the (negative) surface pressure anomalies associated with the Niños in the west European sector in a future climate. This feature is related to the important stratospheric anomalies in the same region, revealed by previous studies.

Citation: OrtizBeviá, M. J., I. Pérez-González, F. J. Alvarez-García, and A. Gershunov (2010), Nonlinear estimation of El Niño impact on the North Atlantic winter, *J. Geophys. Res.*, *115*, D21123, doi:10.1029/2009JD013387.

1. Introduction

[2] A number of recent studies evidence the renewed interest in the nonlinear aspects of the atmospheric response to the ENSO signal. Among these nonlinear features, we count the dependence of the atmospheric response on the sign of the ENSO anomalies [*An and Jin*, 2004; *Lin et al.*, 2005] and on the strength of the signal [*May and Bengtsson*, 1998]. Strong or moderate ENSO events influence the areas of North Pacific tropical storm formation and therefore the tropical storm tracks in a different way [*Wang and Chan*, 2002; *Orlanski*, 2005]. ENSO impacts on the North Pacific in winter are well characterized [*McPhaden et al.*, 2006] while the same does not apply to the North Atlantic. This may be due in part to the weakness of the response of the North Atlantic, or to the interference with the Pacific/North America (PNA) pattern, a part of the North Pacific response to ENSO itself, or with the main signal of the basin, the North Atlantic Oscillation or NAO [*Wu and Hsieh*, 2004]. Other researchers highlight the nonstationary characteristics of ENSO teleconnections that are especially important in regions like the eastern Mediterranean [*Mariotti et al.*, 2002] or the Red Sea [*Rimbu et al.*, 2003].

[3] These nonlinear aspects of the atmospheric response in the North Atlantic have been typically studied using composites [e.g., *Pozo-Vázquez et al.*, 2005]. Stratifying warm ENSO events according to their amplitude, and compositing climate variables, *Toniazzo and Scaife* [2006] find a robust response to ENSO in the North Atlantic that changes sign in the central part of the basin as the amplitude of El Niño anomalies increase. This might account for the weakness of the signal identified with linear statistical methods: when the response to strong and to moderate Niños are added together, the signal is canceled. In view of the characteristics of the signal to capture (there is a delay of one month between the peak of the forcing and the extratropical response [*Kumar and Hoerling*, 2003]) selection of the months that represent winter variability in ocean and atmosphere is no small matter [*Bladé et al.*, 2008].

[4] Composites, unfortunately, and in part due to sampling variability, do not allow for a clear attribution to ENSO of the captured atmospheric signal. Together with the response to ENSO, they can include changes of the mean state due to low-frequency signals. The use of nonlinear techniques, like the nonlinear projection using neural networks of *Wu and Hsieh* [2004], have already proved fruitful. *Hsieh et al.* [2006] show, for instance, that the nonlinear teleconnections of both ENSO phases extend much further in the North Atlantic

[1]Department of Physics, University of Alcalá, Alcalá de Henares, Spain.
[2]Scripps Institution of Oceanography, University of California, San Diego, La Jolla, California, USA.

0148-0227/10/2009JD013387

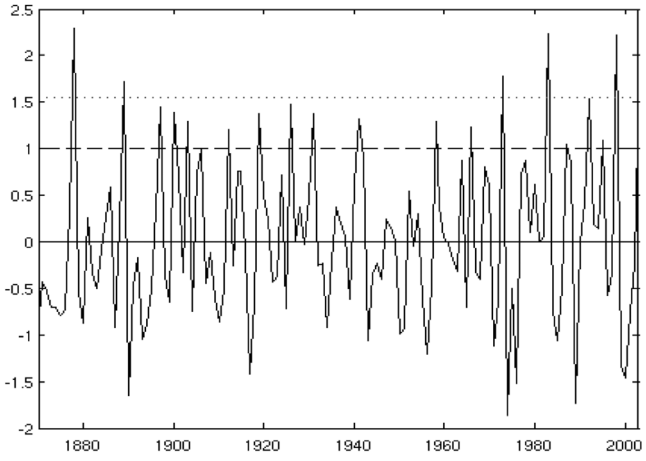

Figure 1. The winter (DJ) Niño3 index from the observations. Event classified as moderate exceeds the value represented with the dashed line. Strong events are those that exceed the 1.5 standard deviation (dotted line). Winters are indexed by the mature event year.

region than do the linear ones. The recent development of a robust version of nonlinear canonical correlation analysis (hereinafter NLCCA [*Cannon and Hsieh*, 2008]), offers a new tool for estimating the atmospheric response with greater confidence.

[5] In this paper, we compare the NLCCA estimate of the atmospheric North Atlantic (hereinafter NA) sector response to Niños of different strengths. Reproducibility of these differences in a coupled control simulation and their modifications in a climate change scenario experiment are also considered. The data and the methods used for the analysis are presented in section 2, the results are displayed in section 3 and discussed in section 4.

2. Data and Methods

[6] The sea surface temperature (SST) data were obtained from the HadISST data set [*Rayner et al.*, 2003] and the mean sea level pressure (SLP) from the HadSLP data set [*Allan and Ansell*, 2004]. Both data sets cover the period 1870 through 2003. The y variables introduced in the first NLCCA analysis are the first 6 Principal Components (PCs) of the standardized winter (JF) anomalies of SLP in the NA sector (20°N – 80°N, 90°W – 40°E) accounting for 80% of the total field variance. The limitation of the atmospheric anomalies under study to the North Atlantic is necessary in view of the characteristics of the El Niño impact on this region compared with the North Pacific. For the x variable we will use basically the first 6 principal components of the standardized winter (DJ) SST anomalies in the tropical Pacific that explain more than 86% of the variability of the original field. Following *Toniazzo and Scaife* [2006], we consider El Niño to occur when the Niño3 index (150°W – 90°W, 5°S – 5°N) exceeds 1 standard deviation, and strong events those above the 1.5 times the standard deviation. In Figure 1 we have represented the December–January Niño3 Index obtained from the observational SST field, with the thresholds for moderate and for strong events depicted by dashed and dotted straight lines respectively. Years are referred to January of the mature year (not to December). Strong events occurred in the years 1878, 1889, 1973, 1983 and 1998.

[7] Our analysis uses basically the simulated pre-industrial SST and SLP data from 500 years of a control simulation with the coupled GFDL model version CM2.1 [*Delworth et al.*, 2006] with greenhouse gas concentrations held fixed at 1860 levels. Future SST and SLP data are from a climate change simulation of 240 years with concentrations varying as observed between 1861 and 2000 and then following the SRESA2 scenario during the 21st century [*Intergovernmental Panel on Climate Change* (*IPCC*), 2007]. The model counts among those of the various of the IPCC ensemble with realistic ENSO simulation and among the few with realistic ENSO teleconnections [*van Oldenborgh et al.*, 2006]. In the case of the control simulation the DJ Niño3 Index is displayed in Figure 2, and in Figure 3 we represent the original scenario Niño3 Index (dotted line) and the same Index computed from the detrended field (solid line). The trend was removed using a nonlinear detrending filter and the analysis for the climate change case was carried out on the detrended field. Occasionally, zonal wind at 200hPa height (hereinafter U200) data from both simulations, and subject to the same treatment were used for the discussion.

[8] Principal Components were computed from the winter seasonal means obtained from the anomalous fields, detrended in the case of the scenario simulation. As in the case of the observations, only the first 6 PC were retained. These explain roughly 80% of the SST, 70% of SLP and 80% of U200 variances field for both the control and the scenario experiments.

[9] In this study we use the robust Nonlinear Canonical Correlation Analysis (NLCCA) version of *Cannon and Hsieh* [2008]. This version keeps the basic model architecture of *Hsieh* [2000] (three feed-forward neural network mappings, as represented in Figure 4) while using a more robust version

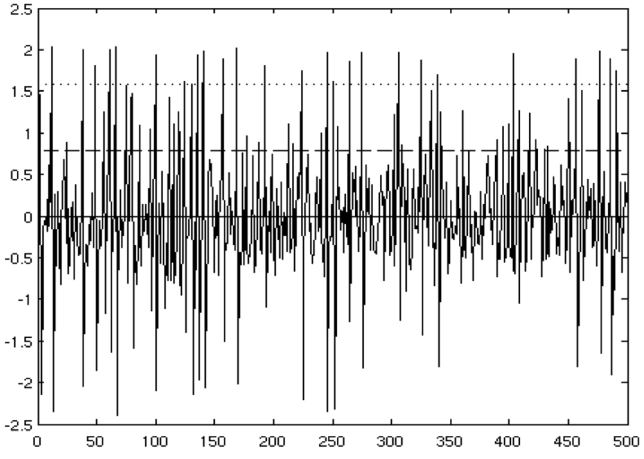

Figure 2. The winter Niño3 index from the control simulation with the GFDL CM2.1 coupled model (winters of years of control simulation given on bottom axis). The thresholds used to classify a warm event as moderate or strong are represented by a straight line, dashed in the case of the moderate events and dotted for the strong events. Years are as in Figure 1.

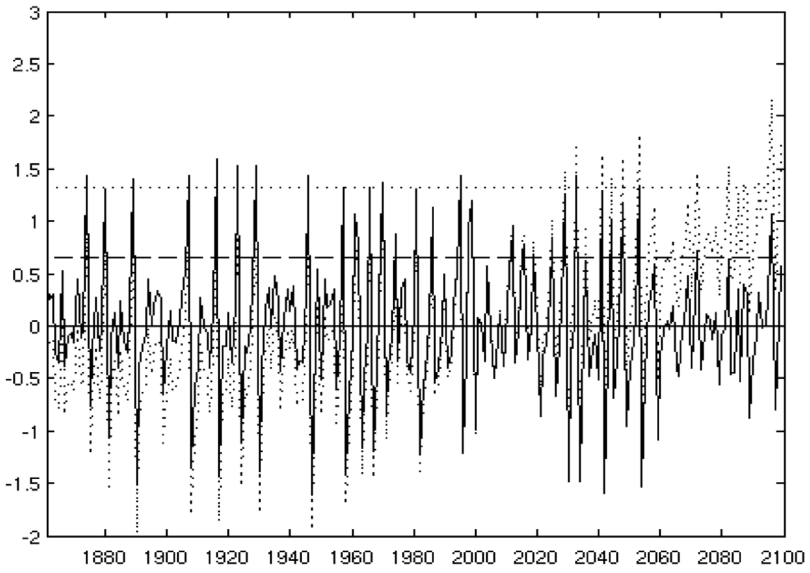

Figure 3. The winter Niño3 index from the climate of the future simulation with the GFDL CM2.1 coupled model (dotted line). The Niño3 Index of the detrended data field is represented with a solid line. As in Figure 2, the thresholds are represented with a straight line, dashed for moderate events and dotted for strong.

of the cost function to set the model parameters. We will give here a brief outline and refer the reader to the original paper for a complete description. Given N samples (fields observed at N different times) of the multivariate data vectors $\mathbf{x}(t)$ and $\mathbf{y}(t)$, the linear CCA version looks for the combinations

$$u(t) = \mathbf{a}\mathbf{x}(t), \quad v(t) = \mathbf{b}\mathbf{y}(t)$$

that maximizes the linear (Pearson) correlation (cor(u,v)) between the canonical variables u and v.

[10] In the nonlinear CCA version we have nonlinear mappings, performed with neural networks, as reflected in the expressions

$$h_k^x = \tanh\left[\left(\mathbf{W}^{(x)}\mathbf{x} + \mathbf{b}^{(x)}\right)_k\right], u = \mathbf{w}'^{(x)}\mathbf{h}^x + b'^{(x)}$$

$$h_l^y = \tanh\left[\left(\mathbf{W}^{(y)}\mathbf{y} + \mathbf{b}^{(y)}\right)_l\right], v = \mathbf{w}'^{(y)}\mathbf{h}^y + b'^{(y)}$$

where h_k^x and h_l^y are the nodes, $\mathbf{W^x}$ and $\mathbf{W^y}$ the weights, tanh(.) is the nonlinear function, $\mathbf{b^{(x)}}$ and $\mathbf{b^{(y)}}$ the bias of the hidden

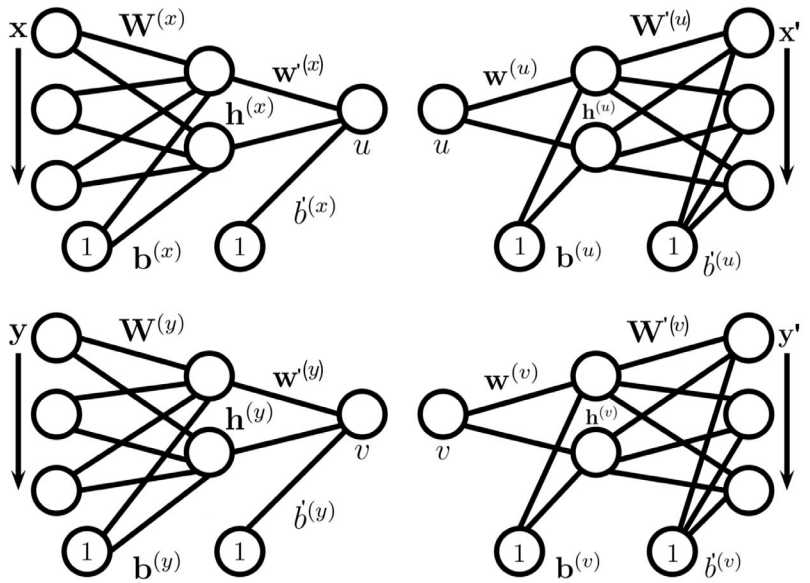

Figure 4. The scheme of the neural network outlay used for the NLCCA computation. (left) The network maps the input variables x and y into u and v, the hidden variables, and (right) u and v are mapped back to x′ and y′.

layer, while $\mathbf{w'^x}$ y $\mathbf{w'^y}$ and $b'^{(x)}$ and $b'^{(y)}$ are weights and bias of the output layers, respectively. The hyperbolic function tanh(.) introduces the nonlinearity in the model; replacing tanh(.) by 1 yields the linear model.

[11] The parameters are obtained by minimizing a cost function that includes the biweight midcorrelation (hereinafter bicor) between two new variables $\mathbf{x}_b$ and $\mathbf{y}_b$. The bicor provides a measure of the association between two variables that is less sensitive to outliers and therefore more robust. If we center $\mathbf{x}(t)$ and $\mathbf{y}(t)$ by M_x and M_y i, the median values of $\mathbf{x}$ and $\mathbf{y}$, then

$$\mathbf{x}^*(t) = \mathbf{x}(t) - M_x$$

$$\mathbf{y}^*(t) = \mathbf{y}(t) - M_y$$

and we rescale the variables with G_x and G_y, the median values of the centered variables

$$p(t) = \frac{\mathbf{x}^*(t)}{9G_x}$$
$$q(t) = \frac{\mathbf{y}^*(t)}{9G_y}.$$

Let define the expressions

$$a(t) = \begin{cases} 0 & |p(t)| > 1 \\ 1 & 0 \le |p(t)| \le 1 \end{cases} \qquad b(t) = \begin{cases} 0 & |q(t)| > 1 \\ 1 & 0 \le |q(t)| \le 1 \end{cases}$$
$$c(t) = 1 - p(t)^2; \qquad d(t) = 1 - q(t)^2$$

then we can write the sample biweight midcovariance as

$$BV(\mathbf{x},\mathbf{y}) = \frac{N \sum_t a(t)b(t)c^2(t)d^2(t)x^*(t)y^*(t)}{\left(\sum_t a(t)c(t)(1-5p^2(t))\right)\left(\sum_t b(t)d(t)(1-5q^2(t))\right)}$$

and the sample biweight midcorrelation

$$BC(\mathbf{x},\mathbf{y}) = \frac{BV(\mathbf{x},\mathbf{y})}{\sqrt{BV(\mathbf{x},\mathbf{x})BV(\mathbf{y},\mathbf{y})}}$$

Details of this derivation are given by *Bishop* [1995]. Additionally, a normalization constraint and a weight penalty controlled by the parameter P_1 arbitrarily chosen, will be also used.

[12] The expressions for the two neural networks that map the u,v variables into $\mathbf{x}'$,$\mathbf{y}'$ can be obtained by replacing in the expressions for h_k^x and h_l^y the ($\mathbf{x}$,$\mathbf{y}$) by (u,v), and the (u,v) by the new ($\mathbf{x}'$,$\mathbf{y}'$). The new weights $\mathbf{w}$ and $\mathbf{W}'$ and bias parameters are set by minimizing the distance functions

$$C_2 = <\| \mathbf{x}' - \mathbf{x} \|^2> + \mathbf{P}_2 \sum_k \left(\mathbf{w}_k^u\right)^2$$

$$C_3 = <\| \mathbf{y}' - \mathbf{y} \|^2> + \mathbf{P}_3 \sum_l \left(\mathbf{w}_l^v\right)^2$$

where, once again, we have to choose the control parameters P_2 and P_3. Once the first mode has been extracted from the data, we obtain the next leading mode from the model residuals, and so on for higher modes. The analysis is stopped when an interpretation of the mode as a coupled feature is not supported by a too low correlation between its time coefficients, or by the lack of significance or robustness of the patterns.

[13] Estimation with the NLCCA model proceeds in two steps. At first, the time series are divided into training and testing intervals. Given the nonlinear nature of the technique, different training and testing intervals leave us with an ensemble of models. Only those among them with similar skill in the training and testing sets are retained to form a reduced ensemble, from which the final estimate is produced by averaging. The quality of the analysis is assessed through the correlation between the time coefficients of the coupled modes (i.e., coupling strength), the significance of the patterns (assessed by a sign t test against the original data) and the amount of variance of the original fields explained. To evaluate the performance of the technique, we will compare the patterns for strong and for moderate ENSO events, produced with the linear and the nonlinear models, with those obtained by compositing the original data.

3. Results

[14] The spatial patterns of the (DJ) SST and the (JF) SLP anomalies for the first mode of the NLCCA analysis of the observations are represented in Figure 5. In Figure 5 (top) the SST (SLP) pattern corresponding to the Niños is depicted in the left (right) column. In Figure 5 (bottom) the SST (SLP) patterns of the Niñas are represented (same distribution). Inspecting Figure 5, one of the conceptual advantages of the nonlinear analysis against the linear one becomes apparent: the spatial pattern that represents the negative forcing of the tropical Pacific SST anomalies (La Niña) is not just the reverse of the one representing the positive forcing (El Niño), and the same applies to the NA response. There are differences in intensity and also in the spatial distribution of the anomalies, as happens between the observed El Niño and La Niña patterns of SST anomalies. Notice, for example, in the case of el Niño pattern how the zero contour stops in the west tropical Pacific, not reaching Indonesia as it does in the La Niña case. In the case of the NA response, differences in the locations of the two maxima of opposite sign, high versus low, are also noticeable (Figure 5, right). The value of the linear correlation between the u and v coefficients of the first mode is 0.59 (0.61 for the bicor used in the cost function), and 0.36 (0.4) in the case of the second mode. The values of the correlations obtained in the linear analysis are 0.56 for the first mode and 0.32 for the second mode. Higher modes are discarded in the reconstruction of the field by the lack of significance of the correlation between time coefficients, or the lack of significance or robustness of the spatial patterns. Hereinafter, the reconstruction of the field with the two leading modes of the linear and of the nonlinear analyses, that is used through this paper, will be mentioned as 'the CCA reconstruction' or the 'NLCCA reconstruction' and the composites computed from those fields, 'the CCA' or the 'NLCCA' composites. The composites of the standardized SLP observations for strong, for moderate, and for all the El Niño events shown in Figure 6 are the same as those of

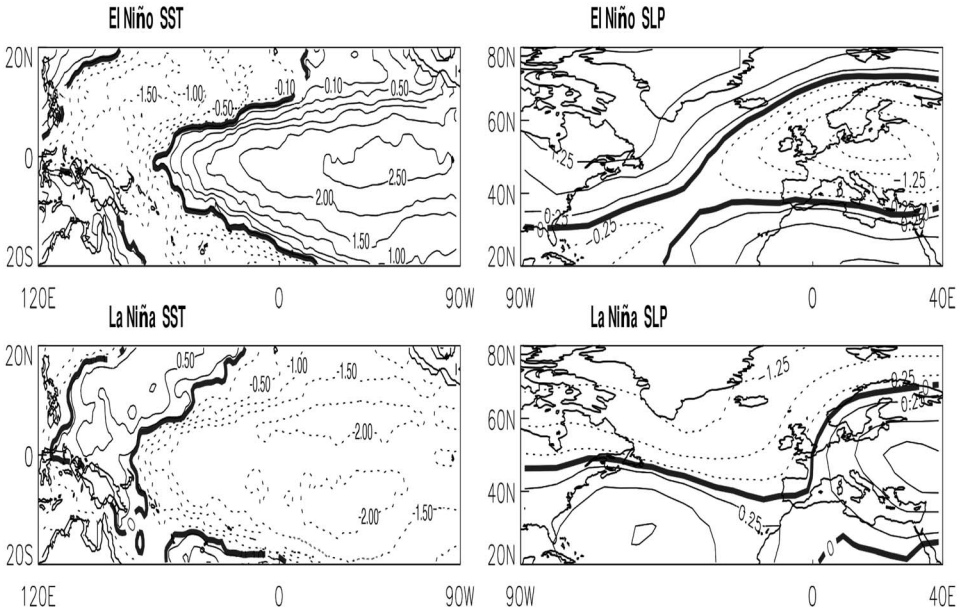

Figure 5. Spatial patterns of (left) SST and (right) SLP anomalies of the first mode of the NLCCA analysis of the tropical Pacific SST and tropical Atlantic SLP anomalies. Contour intervals are 0.5 °C for the SST and 0.25 standardized units for the SLP. Notice the differences in intensity and in the location of the center of action between (top) the positive SST pattern and its associated SLP pattern and (bottom) the negative SST and its associated SLP patterns, an observed feature that is reproduced in the analysis through the use of the nonlinear technique.

Toniazzo and Scaife [2006]. For strong events, the CCA and the NLCCA composites reproduce acceptably the strip of high pressure across the domain of the observed composite. In the case of the moderate events, both linear and nonlinear analysis capture well the atmospheric response, projecting onto the negative North Atlantic Oscillation (NAO) pattern. Regions where the variability is found statistically different from those of normal years by a rank test at the 95% confidence level are shaded. The percent of the variance of the observations explained by the statistical model is represented in Figure 7. The most striking feature of Figure 7 is the differences between the patterns and the corresponding composites. However, notice how, for some regions the NLCCA model explains higher variance than the linear CCA one (e.g., a 20% more in the western Mediterranean).

[15] Most of the moderate events have low-pressure anomalies to the west of Europe, often accompanied by high-pressure anomalies around Iceland and the Arctic. A connection between El Niño events and the negative phase of the NAO was established by *Davies et al.* [1997]. The ENSO-Europe teleconnections follow in part the stratospheric pathway [*Thompson et al.*, 2002; *Douville*, 2009]. During a moderate El Niño event, weaker stratospheric easterlies appear, leading to negative SLP anomalies. On the other hand, strong Niños events produce, compared to moderate ones, proportionally larger SST anomalies in the eastern Pacific. *Li et al.* [2006] have shown that East Pacific SST anomalies are not effective in exciting an annular response in the northern extratropics. To this could contribute the strength of the atmospheric response induced in the northern part of the American continent, with a ridge of high pressures that extend into the Atlantic.

[16] In the case of the control climate simulation, the values of the (linear) correlation among the time coefficients of the two first modes of the nonlinear and the linear analyses are very similar to those found in the analysis of the observations. The corresponding spatial patterns for tropical Pacific SST and the North Atlantic SLP anomalies are represented in Figure 8. The standardized SLP composites for strong and moderate warm ENSO events obtained from the analysis of SLP-SST anomalies appear in Figure 9. For strong El Niño events, the NLCCA composite compares more favorably with the simulated one than the composite produced with the linear CCA. In the case of the moderate events, the composite obtained from the field reconstructed with the two first NLCCA modes is also in good agreement with the one obtained directly from the simulated SLP anomalies. The former captures the two center of low pressure, the one adjacent to the Caribbean and the other located in the Mediterranean region, to be found in the pattern obtained directly from the simulation.

[17] To test if this performance is related to the better statistical sampling provided by the time series length (almost four times the length of the observational record), a number of tests have been conducted. Using a bootstrap procedure [*Efron and Tibishirani*, 1986], we divided the time series of both SST and SLP principal components (the x and y of the CCA model), into a number of subseries going from two (249 year time series) to five (99 year time series) and identified the NLCCA model (or the CCA model) from each of the subseries. We then considered the evolution of the relevant estimation diagnostics (e.g., correlation between the inner u and v variables, cor(u,v), or the errors in the x and y projections (hereinafter Errx and Erry, respectively)). For the cases

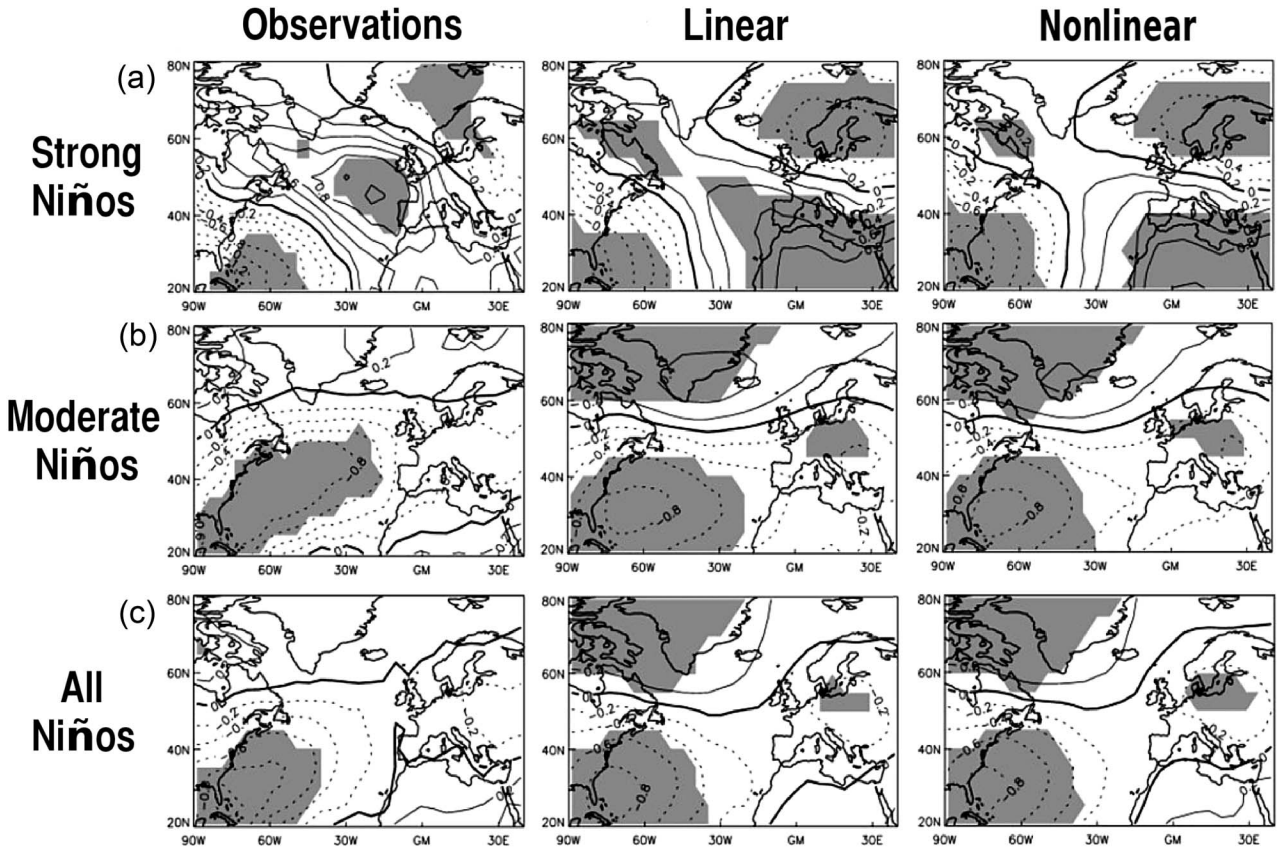

Figure 6. Composites of SLP observed anomalies for (a) strong, (b) moderate, and (c) all ENSO warm events. The composites are obtained (left) directly from the observations, (middle) from the reconstruction with the linear model, and (right) from the reconstruction with NLCCA. Regions where the variability is statistically different from those of normal years at the 95% confidence level are shaded. Contour interval is 0.2 (standardized units).

considered, the NLCCA performances in identifying the first mode is superior to that of the CCA, that is the cor(u,v) in the NLCCA is higher than that from the CCA and the Errx and Erry are lower. It is also important for our analysis to realize that the first EOF, whose coefficient (PC) closely match the Niño3 Index, is the one making the most important contribution to the first mode. On the contrary, in the case of the second mode, model diagnostics are sensitive to the time series length in a way that makes the cor(u,v) determined for the NLCCA mode-2 barely higher that the cor(u,v) of the CCA mode-2, and this up to a time length of roughly 200 years. Moreover, it seems, the cor(u,v) characterizing the second CCA mode is stronger than the corresponding one for the NLCCA. In the case of the second mode, the EOFs lower than first make an important contribution to this mode, and therefore features that are associated with EOFs higher than first are best captured by the CCA model. Such is the case of the high-pressure band across the domain in the observed strong events composite.

[18] The composites of SLP anomalies for the scenario simulation are shown in Figure 10. In the NLCCA composite for the strong events, there is a displacement of the second low toward northwestern Africa (Morocco), compared with its position in the control composite. In the case of the composite for moderate events, the second low is displaced from the Mediterranean to the Euro-Atlantic sector. The generation of the surface atmospheric anomalies in the European sector is closely related to those of its middle atmosphere counterpart, a feature confirmed by the good agreement of the SLP analysis with those of the U200 anomalies (not shown) for the control simulation. In this simulation of a future climate, the intensity of the moderate El Niño events is enhanced with respect to control, a conclusion supported by the inspection of Figure 3 and its comparison with Figure 2. Consistently, the maximum value of the SLP (detrended) patterns for the first mode of the NLCCA analysis of the scenario anomalies, represented in Figure 10, is increased during the moderate Niños. Changes in the upper level wind fields are consistent with these surface changes. The NLCCA SLP composite shows an increased ENSO impact on the NA sector concealed in part in the scenario simulation by the changes in the mean state induced by increased GHG concentrations. Indeed, changes in tropical Pacific SST induce changes in the Walker and Hadley circulations. In the GFDL simulation, as in the ECHAM5/MPI-OM [*Mueller and Roeckner*, 2008], there is an anomalous inverse Hadley circulation, that produces high pressures over Mexico and the southern USA. The anomalous subtropical low in the Atlantic sector, connected to anomalous SST in the Niño3 region is then displaced

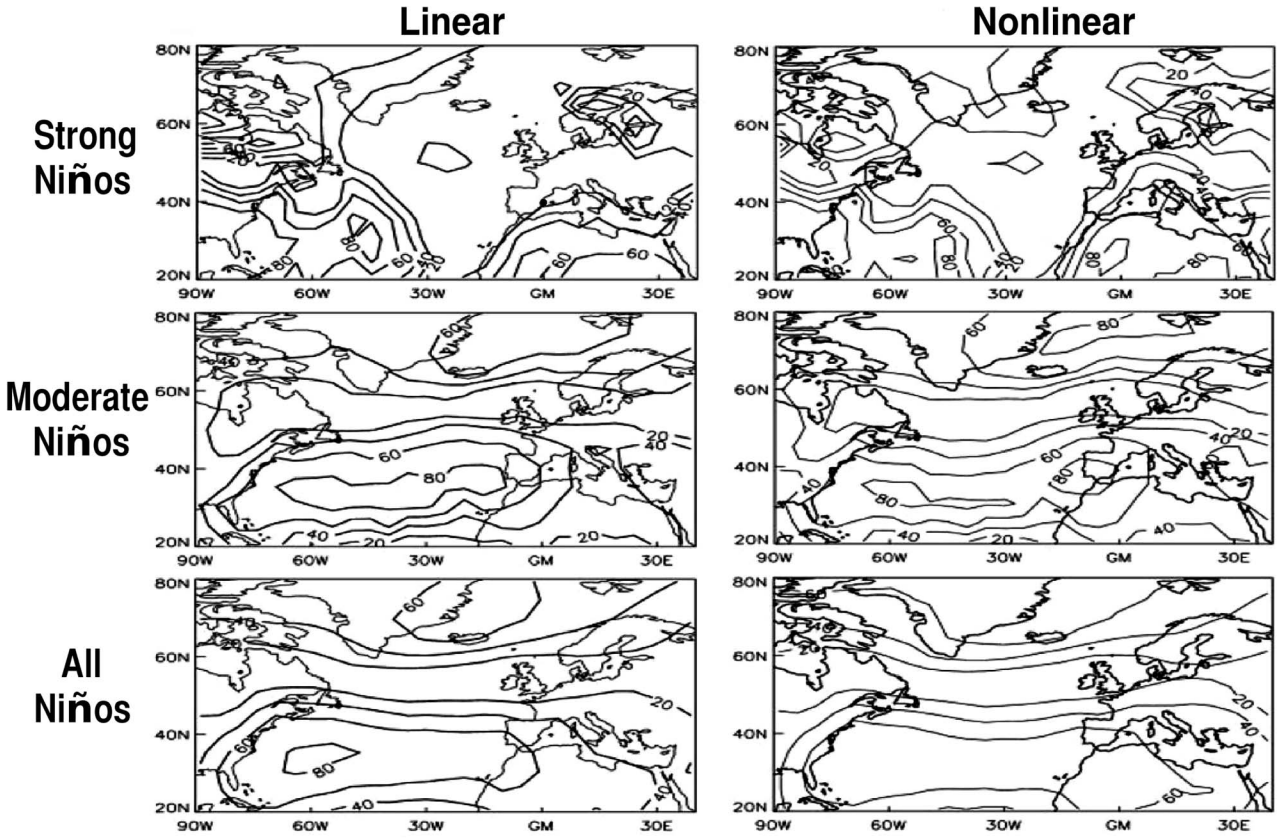

Figure 7. The variable represented here is the percent of the SLP anomalous field variance from the observations explained by the statistical model, (left) with the linear and (right) with the nonlinear models. (top) The case of strong ENSO warm events, (middle) the moderate ones, and (bottom) the variance explained for all the ENSO events. Contour interval is 20% of explained variance.

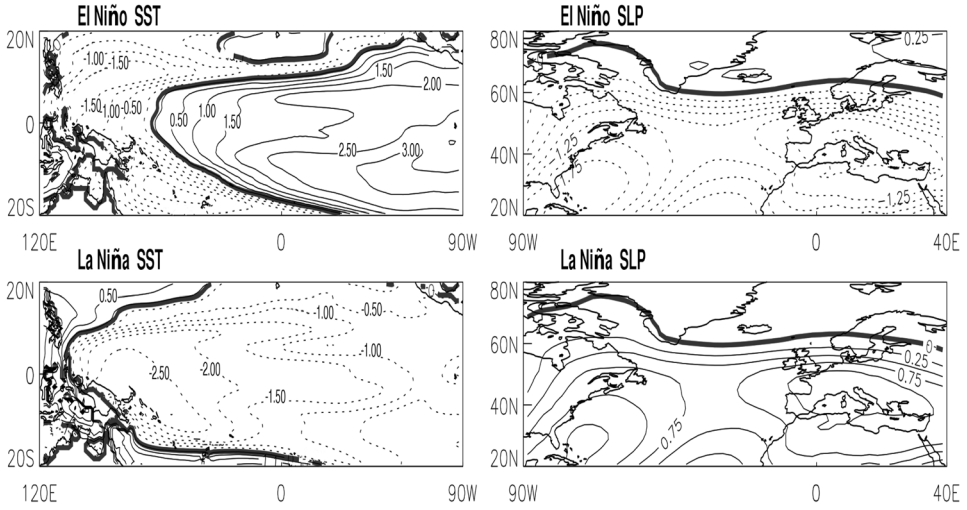

Figure 8. Spatial patterns of (left) SST and (right) SLP anomalies of the first mode of the NLCCA analysis of those variables in the GFDL CM2.1 control simulation. (top) The positive SST pattern and its atmospheric response and (bottom) the negative one. These plots are to be compared with Figure 5, where the patterns obtained from the observations are depicted. Contour intervals are 0.5°C for the SST and 0.25 standardized units for the SLP.

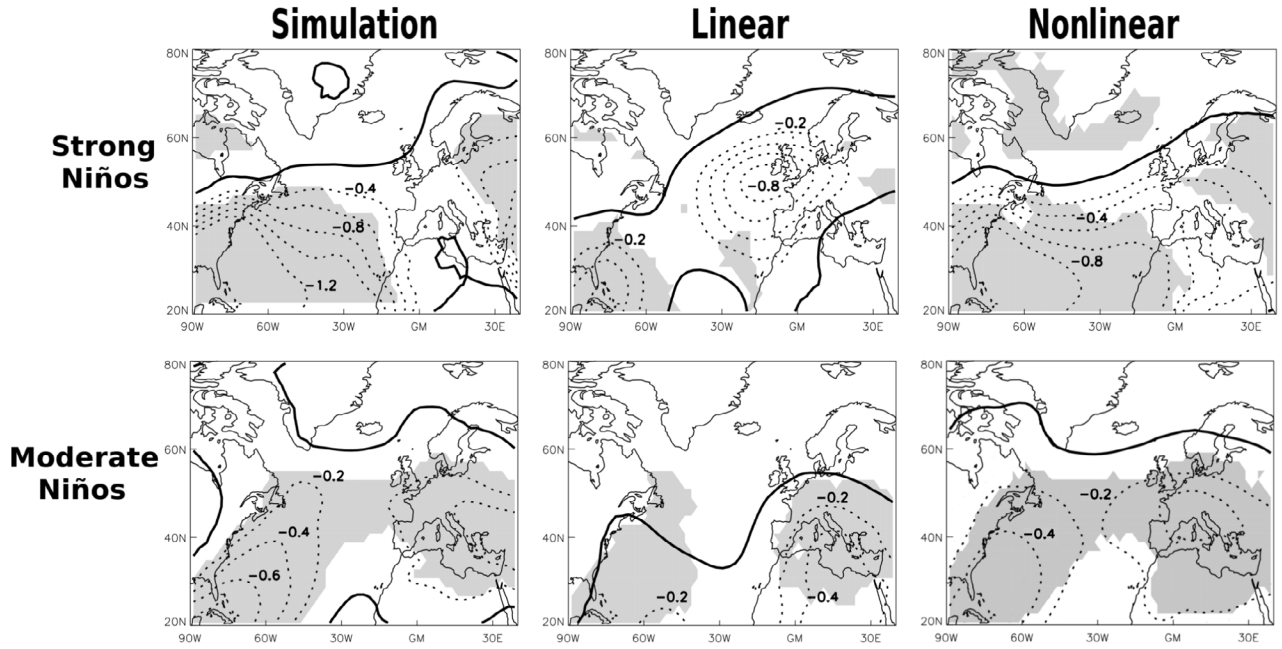

Figure 9. Composites of SLP anomalies for (top) strong and (bottom) moderate ENSO warm events in the control experiment. (left) The simulation composites, (middle) the CCA reconstruction, and (right) the NLCCA results. Regions where the variability is statistically different from those of normal years at the 95% confidence level are shaded. Contour interval is 0.2 (standardized units).

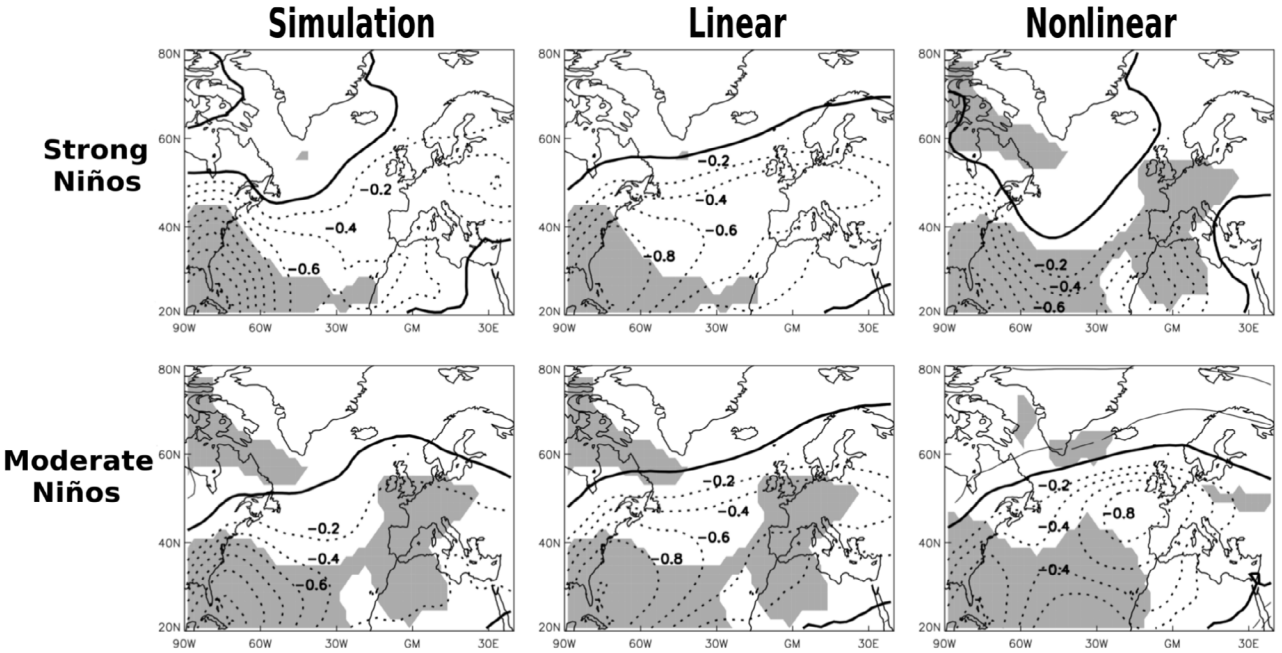

Figure 10. Composites of SLP anomalies for (top) strong and (bottom) moderate ENSO warm events in the scenario experiment (standardized units). (left) The simulation composites, (middle) the CCA reconstruction, and (right) the NLCCA results. Regions where the variability is statistically different from those of normal years at the 95% confidence level are shaded. Contour interval is 0.2 (standardized units).

toward the central Atlantic and therefore more strongly affects the European sector.

4. Conclusion and Discussion

[19] When moderate ENSO events take place, the North Atlantic atmospheric anomalies present a number of common traits. These are missing in the North Atlantic anomalies of strong ENSO events. The characteristics of the response (and not only its strength) seem to be dependent on the strength of the forcing (the ENSO signal). It is appropriate to use a nonlinear technique to study a nonlinear behavior. The NLCCA has already proved its advantages at estimating the response of the tropical atmosphere to ENSO, and at forecasting it. We validate the results of the NLCCA analysis with statistical tests and evaluate its performance by reference to the response estimated by the traditional linear CCA and by compositing.

[20] In the case of the observations, the performance of the linear and of the nonlinear statistical CCA model at capturing the main differences between the atmospheric response to strong and to moderate ENSO events is similar. However, the reconstruction with the NLCCA model explains a greater amount of the total observed variance for some regions, like the western Mediterranean region. Importantly, the NLCCA provides a conceptual frame that is more satisfactory at representing both the tropical forcing and the North Atlantic, because it provides a more appropriate representation of the real world, by allowing for differences among the negative and the positive patterns that represent the maximum value of both, the forcing and its atmospheric impact.

[21] We compare the results of the analysis performed on the observations with those of the control experiment of a realistic GCM simulation of climate variability. The length, and other characteristics (e.g., stationarity, data availability of poorly observed variables) of the control simulation allows for a more complete statistical determination than the one provided by the observations. The composites estimated with the NLCCA reconstruction compare better with the ones obtained directly from the simulated fields than the ones obtained from the CCA analysis, for both strong events and moderate events. Two physical mechanisms at play here can explain these differences in the response. The characteristics (location, etc.) of the tropical storms (TS) generation areas in the tropical North Pacific are known to be sensitive to the forcing strength [*Wang and Chan*, 2002]. In late fall of El Niño development years, the observed TS formation areas are displaced toward the southeast. The mean displacement is more than 9 degrees in longitude in the case of strong Niños, and less than 1 degree for moderate Niños. The differences in the poleward air fluxes will produce differences in their interaction with the Aleutian low, and in the tropospheric response in the Pacific-North America region [*Orlanski*, 2005]. Moreover, changes in the convection areas of the tropical Pacific will produce changes in the stratosphere, that will propagate toward higher latitudes and induce there baroclinic processes that subsequently will modify the upper layer zonal winds [*Douville*, 2009]. Then, at higher latitudes, the tropospheric and the stratospheric teleconnections will interact. Numerical experiments [*Bell et al.*, 2009] show that in the case of moderate Niños, the influence of the stratospheric teleconnection on the surface variables at polar latitudes is clear, while in the case of strong Niños it is blurred by other processes.

[22] The impact of strong Niños events of the scenario simulation has more traits in common with its observational counterpart than with that of the control experiment. The analysis of the scenario simulation presented here suggests that ENSO impact in the North Atlantic sector, for strong and moderate events, will increase in the future. This increased influence can be explained by the modifications in the stratospheric state [*Santer et al.*, 2003] and in the North Pacific TS formation areas [*Wu and Wang*, 2004] revealed by analyses of observations and simulations. This feature agrees also well with *Mueller and Roeckner's* [2008] analysis using the ECHAM5/MPI-OM model. It is also in good accord with the observation by [*Meehl and Teng* 2007], who pointed to an influence of ENSO on the upper tropospheric wind anomalies, as a common trait among a subset of the IPCC AR4 models, characterized by increasing ENSO amplitude, to which the simulation analyzed here belong. Our results are also consistent with an important role of the stratosphere in channeling ENSO teleconnections to Europe, a role that will be the focus of a forthcoming study.

[23] **Acknowledgments.** M. Cannon and W. Hsieh are acknowledged for the NLCCA code available at the Web page http://www.ocgy.ubc.ca/~william. Thanks are owed also to two anonymous reviewers for their contribution to the discussion of the results. We also thank J. Hernández Carretero for his help with the files and the Matlab programming. This work was financed by the Spanish MICINN under project CGL2006–09268. The University of Alcalá also provided funding for both A. Gershunov and M. OrtizBevia, at different stages through this work.

References

Allan, R. J., and T. J. Ansell (2004), A new globally complete monthly historical mean sea level pressure dataset (HadSLP2) 1850–2004, *J. Clim.*, *53*, 5816–5842.

An, J. L., and F. F. Jin (2004), Nonlinearity and asymmetry of ENSO, *J. Clim.*, *17*, 2399–2412.

Bell, C. J., L. J. Gray, A. J. Charlton-Perez, M. M. Joshi, and A. A. Scaife (2009), Stratospheric communication of El Niño teleconnections to European winter, *J. Clim.*, *22*, 4083–4096.

Bishop, C. M. (1995), *Neural Networks for Pattern Recognition*, Oxford Univ. Press, Oxford, U. K.

Bladé, I., M. Newman, M. A. Alexander, and J. D. Scott (2008), The late fall extratropical response to ENSO: Sensitivity to coupling and convection in the tropical West Pacific, *J. Clim.*, *21*, 6101–6118.

Cannon, M., and W. Hsieh (2008), Robust nonlinear canonical correlation analysis: Application to seasonal climate forecasting, *Nonlin. Processes Geophys.*, *15*, 221–232.

Davies, J. R., D. P. Rowell, and C. K. Folland (1997), North Atlantic and European seasonal predictability using an ensemble of multidecadal atmospheric GCM simulations, *Int. J. Climatol.*, *17*, 1263–1284.

Delworth, T. L., et al. (2006), GFDL's CM2 global coupled climate model. Part 1, Formulation and simulation characteristics, *J. Clim.*, *18*, 643–674.

Douville, H. (2009), Stratospheric polar vortex influence on Northern Hemisphere winter climate variability, *Geophys. Res. Lett.*, *36*, L18703, doi:10.1029/2009GL039334.

Efron, B., and R. Tibishirani (1986), Bootstrap methods for standard errors, confidence intervals and other measures of statistical accuracy, *Stat. Sci.*, *1*, 54–75.

Hsieh, W. (2000), Nonlinear canonical correlaition analysis by neural networks, *Neural Networks*, *14*, 1095–1105.

Hsieh, W. W., A. Wu, and A. Shabbar (2006), Nonlinear atmospheric teleconnection, part I: Methodology and hemispheric regimes, *Geophys. Res. Lett.*, *33*, L07714, doi:10.1029/2005GL025471.

Intergovernmental Panel on Climate Change (IPCC) (2007), *Climate Change 2007: The Physical Science Basis*, edited by S. Solomon et al., Cambridge Univ. Press, Cambridge, U. K.

Kumar, A., and M. P. Hoerling (2003), The nature and causes for the delayed atmospheric response to El Niño, *J. Clim.*, *16*, 1391–1403.

Li, S., M. P. Hoerling, S. Peng, and K. M. Weickmann (2006), The annular response to tropical Pacific SST forcing, *J. Clim.*, *17*, 1802–1819.
Lin, M., M. Derome, and G. Brunet (2005), Tropical Pacific link to the two dominant patterns of atmospheric variability, *Geophys. Res. Lett.*, *32*, L03801, doi:10.1029/2004GL021495.
Mariotti, A., N. Zeng, and K. M. Lau (2002), Euro-Mediterranean rainfall and ENSO—A seasonally varying relationship, mean flow and high frequency intraseasonal variability, *Geophys. Res. Lett.*, *29*(12), 1621, doi:10.1029/2001GL014248.
May, W., and L. Bengtsson (1998), The signature of ENSO in the Northern Hemisphere mid-latitude seasonal mean flow and high frequency intraseasonal variability, *Meteorol. Atmos. Phys.*, *69*, 81–100.
McPhaden, M. J., S. E. Zebiak, and M. H. Glantz (2006), ENSO as an integrating concept in Earth sciences, *Science*, *314*, 1740–1745.
Meehl, G. A., and F. Teng (2007), Multi-model changes in El Niño teleconnections over North America in a future warmer climate, *Clim. Dyn.*, *29*, 779–790.
Mueller, W. A., and E. Roeckner (2008), ENSO teleconnections in projections of future climate in ECHAM5/MPI-OM, *Clim. Dyn.*, *31*, 533–549.
Orlanski, I. (2005), A new look at the Pacific storm track variability: Sensitivity to tropical SSTs and to upstream seeding, *J. Clim.*, *62*, 1367–1390.
Pozo-Vázquez, D., S. R. Gamiz-Fortis, J. Tovar-Pescador, M. J. Esteban-Parra, and Y. Castro-Díez (2005), North Atlantic winter SLP anomalies based on the Autumn ENSO state, *J. Clim.*, *18*, 97–103.
Rayner, N. A., et al. (2003), Global analyses of sea surface temperature, sea ice and night marine air temperature since the late nineteenth century, *J. Geophys. Res.*, *108*(D14), 4407, doi:10.1029/2002JD002670.
Rimbu, N., G. Lohman, T. Felis, and J. Paetzold (2003), Shifts in ENSO teleconnections recorded by a Red Sea Coral, *J. Clim.*, *16*, 1414–1422.
Santer, B. D., et al. (2003), Contribution of anthropogenic and natural forcing to recent tropopause height changes, *Science*, *301*, 479–493.
Thompson, D. W. J., M. P. Baldwin, and J. M. Wallace (2002), Stratospheric connection to Northern Hemisphere wintertime weather: Implications for prediction, *J. Clim.*, *15*, 1421–1428.
Toniazzo, T., and A. A. Scaife (2006), The influence of ENSO on winter North Atlantic climate, *Geophys. Res. Lett.*, *33*, L24704, doi:10.1029/2006GL027881.
van Oldenborgh, G. J., S. Phillip, and M. Collins (2006), El Niño in a changing climate: A multimodel study, *Ocean Sci.*, *20*, 565–574.
Wang, B., and J. C. Chan (2002), How strong ENSO affect tropical storm activity over the western North Pacific, *J. Clim.*, *15*, 1643–1658.
Wu, A. M., and W. W. Hsieh (2004), The nonlinear northern hemisphere winter atmospheric response to ENSO, *Geophys. Res. Lett.*, *31*, L02203, doi:10.1029/2003GL018885.
Wu, L., and B. Wang (2004), Assessing impacts of global warming on tropical cyclone tracks, *J. Clim.*, *17*, 1686–1698.

F. J. Alvarez-García, M. J. OrtizBeviá, and I. Pérez-González, Department of Physics, University of Alcalá, Carretera de Barcelona, Km 33.6, E-28871 Alcalá de Henares (Madrid), Spain. (mjose.ortiz@uah.es)
A. Gershunov, Scripps Institution of Oceanography, University of California, San Diego, La Jolla, CA 92093 USA.